

## Structure-Based de Novo Design, Synthesis, and Biological Evaluation of Non-Azole Inhibitors Specific for Lanosterol 14 $\alpha$ -Demethylase of Fungi

Haitao Ji,<sup>\*,†</sup> Wannian Zhang,<sup>†</sup> Min Zhang,<sup>‡</sup> Makiko Kudo,<sup>§</sup> Yuri Aoyama,<sup>||</sup> Yuzo Yoshida,<sup>§</sup> Chunquan Sheng,<sup>†</sup> Yunlong Song,<sup>†</sup> Song Yang,<sup>†</sup> Youjun Zhou,<sup>†</sup> Jianguo Lü,<sup>†</sup> and Jü Zhu<sup>†</sup>

School of Pharmacy and Department of Microbiology, Second Military Medical University, Shanghai 200433, China, School of Pharmaceutical Sciences, Mukogawa Women's University, Nishinomiya 663-8179, Japan, and Faculty of Engineering, Soka University, Hachioji, Tokyo 192-8577, Japan

Received August 20, 2002

The active site of lanosterol 14 $\alpha$ -demethylase (CYP51) was investigated via MCSS functional group mapping and LUDI calculations. Several non-azole lead molecules were obtained by coupling structure-based de novo design with chemical synthesis and biological evaluation. All of the lead molecules exhibited a strong inhibitory effect on CYP51 of *Candida albicans*. They occupy the substrate-binding site and interfere with the binding of azole antifungal agents in a competitive manner. The mode of action of the lead molecules was validated by spectrophotometric analysis and SAR studies. This is the first successful example reported for the inhibitor design of the cytochrome P450 superfamily using the de novo design strategy. Because the affinity of the lead molecules for CYP51 was mainly attributed to their nonbonding interaction with the apoprotein, the studies presented here afford the opportunity to develop novel antifungal agents that specifically interact with the residues in the active site and avoid the serious toxicity arising from coordination binding with the heme of mammalian P450s.

### Introduction

Lanosterol 14 $\alpha$ -demethylase (CYP51) is a member of the cytochrome P450 superfamily, which catalyzes the oxidative removal of the 14 $\alpha$ -methyl group (C-32) of lanosterol to give  $\Delta^{14,15}$ -desaturated intermediates in ergosterol biosynthesis.<sup>1</sup> During the catalytic cycle, a substrate undergoes three successive monooxygenation reactions resulting in the formation of 14-hydroxy-methyl, 14-carboxaldehyde, and 14-formyl derivatives followed by elimination of formic acid with concomitant introduction of a C14, C15 double bond. CYP51 is one of the key enzymes of sterol biosynthesis in different biological kingdoms, such as fungi, higher plants, and mammals, with the same metabolic role, i.e., removal of the 14 $\alpha$ -methyl group of sterol precursors lanosterol and 24(28)-methylene-24,25-dihydrolanosterol in fungi, obtusifoliol in plants, and 24,25-dihydrolanosterol in mammals. This is the only known cytochrome P450 occurring in eukaryotes with essentially the same metabolic role.<sup>2,3</sup>

The development of inhibitors of lanosterol 14 $\alpha$ -demethylase in fungi has provided a rich source of drugs, such as clotrimazole, ketoconazole, fluconazole, and itraconazole (Chart 1).<sup>4</sup> These azole antifungal drugs are classified as imidazole and triazoles on the basis of whether they have two or three nitrogens in the five-membered azole ring. They have fungistatic, orally active, and broad-spectrum activities against most yeasts and filamentous fungi. Azole antifungal agents

inhibit the CYP51 by a mechanism in which the heterocyclic nitrogen atom (N-3 of imidazole and N-4 of triazole) binds to the heme iron atom in the binding site of the enzyme. The resulting ergosterol depletion and the accumulation of precursor 14 $\alpha$ -methylated sterols interfere with the function of ergosterol as a membrane component. They disrupt the structure of the plasma membrane, making it more vulnerable to further damage, and alter the activities of several membrane-bound enzymes.<sup>5,6</sup> Differential inhibition of this cytochrome P450 enzyme between pathogenic fungi and mammals should be the basis for the clinically important activity of azole antifungal agents.<sup>7</sup> However, in fact, azole antifungal agents are generally toxic and are hampered in the treatment of deep-seated mycoses and life-threatening systemic infections because of their ability to coordinate with the heme of a lot of host cytochrome P450 enzymes, particularly mammalian CYP3A4.<sup>8,9</sup> Cases of fatal hepatotoxicity have been reported.<sup>10–15</sup> The azole ring has been demonstrated to be one of the most important pharmacophores for antifungal activity in extensive structure–activity studies,<sup>16,17</sup> and both toxicity and activity of azole antifungal agents are mainly attributed to the coordination binding of the nitrogen atom of the azole ring to the iron atom of heme. All of these findings urged us to learn more about the active site of fungal CYP51 and to search novel non-azole lead compounds with more structural specificity for the fungal enzyme to separate their activity from toxicity.

Because lanosterol 14 $\alpha$ -demethylase represents an attractive target for antifungal therapy, we have constructed a three-dimensional model of CYP51 from *Candida albicans* on the basis of the crystallographic coordinates of four prokaryotic P450s: P450BM3, P450cam, P450terp, and P450eryF in previous studies.<sup>18</sup>

\* To whom correspondence should be addressed. Current address: Department of Chemistry, Northwestern University, 2145 Sheridan Road, Evanston, IL 60208-3113. Phone: 1-847-491-2991. Fax: 1-847-491-7713. E-mail: jihaitao@chem.nwu.edu.

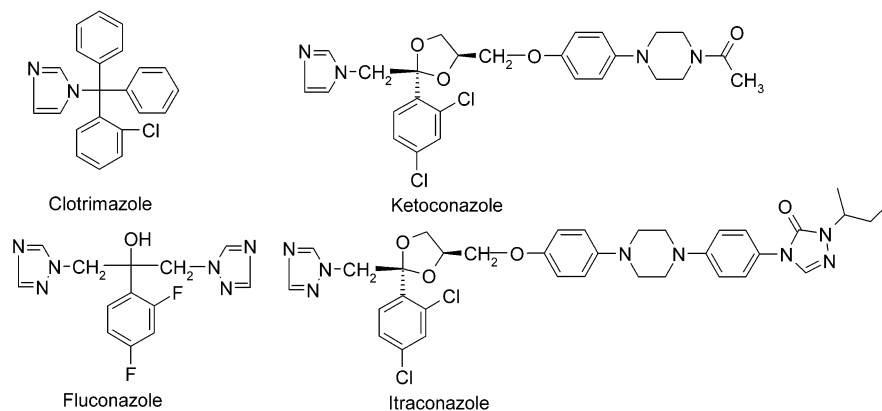
<sup>†</sup> School of Pharmacy, Second Military Medical University.

<sup>‡</sup> Department of Microbiology, Second Military Medical University.

<sup>§</sup> Mukogawa Women's University.

<sup>||</sup> Soka University.

Chart 1



The pharmacophoric conformations of azole antifungal agents were searched by the active analogue approach and docked into the active site of the enzyme. Subsequently, the substrate and azole-binding residues in the active site were identified. Recently, the crystal structure of a prokaryotic sterol 14 $\alpha$ -demethylase from *Mycobacterium tuberculosis* complexed with fluconazole was determined.<sup>19</sup> The binding conformation of fluconazole in the crystal structure was identical to the bioactive conformation identified in our model. The location and mode of action of fluconazole with the enzyme were also similar to that reported in our earlier paper. The N-4 atom of the azole ring of fluconazole coordinated to the iron atom of heme, and the halogenated phenyl ring of the inhibitors was located in the hydrophobic binding cavity lined with residues in the B' helix-meander1 loop and the N terminus of helix I.

The three-dimensional model of lanosterol 14 $\alpha$ -demethylase from *Candida albicans* and the crystal structure of the prokaryotic sterol 14 $\alpha$ -demethylase from *Mycobacterium tuberculosis* provided the basis for the structure-based antifungal drug design. In the present study, the active site of CYP51 was investigated thoroughly and some non-azole antifungal lead compounds were discovered by coupling structure-based de novo design with chemical synthesis and biological evaluation. During the process of inhibitor design, only those functional groups forming noncovalent bonds with the amino acid residues in the active site of CYP51 were introduced. The reliability of the three-dimensional structure of the active site and the mode of action of the lead molecules with the active site of CYP51 were validated by spectrophotometric analysis and structure-activity relationship (SAR) studies. Because the affinity of the lead molecules for CYP51 was mainly attributed to their nonbonded interaction with the apoprotein, our studies presented here demonstrate that it is possible to identify novel antifungal agents that specifically interact with amino acid residues in the active site of lanosterol 14 $\alpha$ -demethylase of fungi and avoid the serious toxicity arising from the coordination binding with the prosthetic group heme, as found in azole antifungal agents.

## Materials and Methods

**Molecular Modeling and Lead Design.** The crystallographic coordinates of sterol 14 $\alpha$ -demethylase from *Mycobacterium tuberculosis* (2.2 Å resolution,  $R_{\text{cryst}} = 0.20$ ) were obtained from the Brookhaven Protein Databank, entry 1EA1.

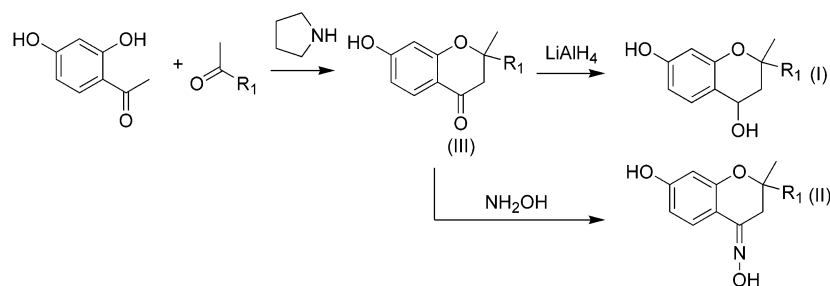
The three-dimensional molecular model of lanosterol 14 $\alpha$ -demethylase from *Candida albicans* was constructed in our previous studies.<sup>18</sup> The molecular modeling was achieved with commercially available InsightII 2000<sup>20</sup> and SYBYL 6.2<sup>21</sup> software packages. The quantum chemistry calculation was carried out using Gaussian 98.<sup>22</sup> All of the computational work was performed on Silicon Graphics workstations (Indigo II and O2). The size and spatial orientation of the active site were identified by the grid analysis implemented in the Binding Site Analysis module within InsightII. The grid size for searching the proteins was set to 1 Å  $\times$  1 Å  $\times$  1 Å. All of the solvent-accessible surfaces in the proteins were filled with grid points and only those having at least 125 grid points were accepted as possible ligand binding sites.

To explore the key regions in the active site that are necessary for ligand binding, the multiple copy simultaneous search (MCSS) program was employed to calculate the energetically favorable position and the orientation of given functional groups in the active site of the enzymes.<sup>23</sup> The functional groups chosen for the MCSS calculation were benzene, propane, cyclohexane, phenol, methanol, ether, and water, representing a hydrophobic functional group, a polar functional group, and solvent. The binding site areas in the MCSS simulation were defined as an approximate 29 Å  $\times$  22 Å  $\times$  26.5 Å box for CYP51 from *Candida albicans* and an approximate 29 Å  $\times$  20 Å  $\times$  24.5 Å box for CYP51 from *Mycobacterium tuberculosis*, which were centered around the grid points searched by InsightII/Binding Site Analysis. Replicas of a given functional group were randomly distributed inside the binding site and then simultaneously and independently energy-minimized. Pairs of molecules were considered to be identical if the root-mean-square deviation (rmsd) between them was less than 0.2 Å, and in such cases, one of the pairs was eliminated. The above protocol was repeated 10 times for each of the functional groups to allow complete searching of the active site. All of the above calculations were performed using the CHARMM 22 force field and MCSS 2.1 program.<sup>24</sup>

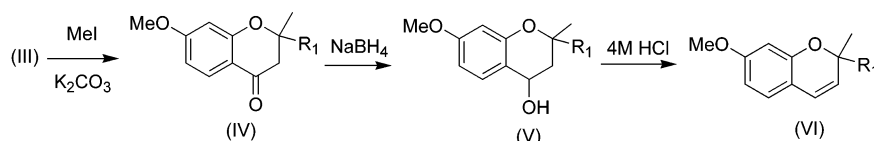
The de novo design program LUDI was employed to further explore the important regions in the active site for ligand binding.<sup>25</sup> The grid points produced by the InsightII/Binding Site Analysis module were divided into four subsites. The residues inside a 6 Å radius sphere, which centered on the centroid of each subsite, were used to generate the interaction site. Three different types of interaction sites are defined in the program: lipophilic, hydrogen bond donor, and hydrogen bond acceptor. The standard default parameter and a fragment library supplied with the program were used during the LUDI search.

The lead molecules were constructed by manually linking some of the MCSS minima.<sup>26</sup> The new bond was constructed so that there was no introduction of significant internal strain in the candidate ligand. The synthetic accessibility of the generated structures was taken into account during the fragment connection step. The newly formed ligand molecules were subsequently energy-minimized in the rigid protein to

## Scheme 1



## Scheme 2



regularize the internal coordinates using the CVFF force field in the Discover 95.0 program within InsightII. The flexible ligand docking procedure in the Affinity module within InsightII was then used to define the lowest energy position for the generated molecules by using a Monte Carlo docking protocol. All of the atoms within a defined radius (6 Å) of the lead molecules were allowed to move. The solvation grid supplied with the Affinity program was used.<sup>27</sup> If the resulting ligand/receptor system was within a predefined energy tolerance of the previous structure, the system was subjected to minimization. The resulting structure was accepted on the basis of an energy check, which used the Metropolis criterion, and also a check of the rms distance of the new structure versus the structure found so far. The final conformations were obtained through a simulation annealing procedure from 500 to 300 K, and then 5000 rounds of energy minimization were performed to reach a convergence, where the resulting interaction energy values were used to define a rank order. Each energy-minimized final docking position of the lead molecules was evaluated using the interaction score function in the LUDI module.<sup>28,29</sup>

**Chemical Synthesis (Schemes 1 and 2).** Infrared spectra (IR) were recorded on a Perkin-Elmer 683 instrument. Mass spectra (MS) were measured on a MAT-212 instrument in the EI mode (70 eV, direct inlet). Nuclear magnetic resonance (NMR) spectra were recorded on a Bruker AC-300p spectrometer with TMS as an internal standard and CDCl<sub>3</sub> as solvent. Elemental analyses were performed with a MOD-1106 instrument.

**General Procedure for the Preparation of 4-Chromanones (III).** A mixture of 2,4-dihydroxyacetophenone (0.03 mol), alkyl methyl ketones (0.03 mol), and pyrrolidine (0.09 mol) was dissolved in 30 mL of absolute ethanol. A total of 5 g of powdered 3 Å molecular sieves was added to the mixture. The mixture was stirred at 25–60 °C for 48–96 h. The reaction was monitored by thin-layer chromatography (TLC). The molecular sieves were removed by filtration and washed with ethanol (2 × 30 mL). The combined organic washings were poured into 1 M HCl and extracted with ether (3 × 50 mL). The extract was washed with ice/water and brine, and dried over MgSO<sub>4</sub>. After evaporation of the solvent, the residue was purified by column chromatography on silica gel (*n*-hexane/EtOAc = 7.25:2.75) to give III as white powders.

**General Procedure for the Preparation of 4,7-Chromanols (I).** A solution of III (0.05 mol) in dry ether (100 mL) was added dropwise to a previously prepared solution of LiAlH<sub>4</sub> (0.01 mol) in 25 mL of dry ether with cooling (–7 to –10 °C). The reaction mixture was then stirred for 12 h at room temperature (TLC monitoring). Ice/water was added dropwise to stop the reaction. A white precipitate was removed by filtration. The solvent was removed by distillation, and the

residue was purified by column chromatography on silica gel (*n*-hexane/EtOAc = 7:3) to give I as white powders.

**General Procedure for the Preparation of 4-Oximinochromanes (II).** A solution of III (0.01 mol) and hydroxylamine hydrochloride (0.02 mol) in 40 mL of absolute ethanol was refluxed at room temperature until all or most of the starting 4-chromanone disappeared by TLC. Following evaporation of the solvent, the residue was taken up with EtOAc and water and the combined organic extracts were washed with water and dried over anhydrous MgSO<sub>4</sub>. After evaporation of the solvent, the residue was purified by column chromatography on silica gel (*n*-hexane/EtOAc = 7:3) to give II as white powders.

**General Procedure for the Preparation of IV.** A mixture containing III (0.01 mol), anhydrous K<sub>2</sub>CO<sub>3</sub> (0.012 mol), 20 mL of dry acetone, and CH<sub>3</sub>I (0.014 mol) was heated gently under reflux for 24 h (TLC monitoring). K<sub>2</sub>CO<sub>3</sub> was removed by filtration and washed with acetone (2 × 20 mL). The combined organic washings were evaporated in a vacuum. The residue was purified by column chromatography on silica gel (*n*-hexane/EtOAc = 8.5:1.5) to give IV as brown oils.

**General Procedure for the Preparation of 4-Chromanols (V).** NaBH<sub>4</sub> (0.01 mol) was added to a solution of IV (0.01 mol) in methanol (30 mL), and the mixture was stirred at room temperature for 2 h. Then an additional equimolecular amount of the hydride was added and stirring was prolonged until the reaction was completed (TLC monitoring). The solvent was removed in a vacuum, and 25 mL of cold water was added. Extraction was performed with ether (3 × 25 mL), and the combined organic extracts were washed with ice/water (3 × 25 mL) and brine and dried over anhydrous Na<sub>2</sub>SO<sub>4</sub>. After evaporation of the solvent, the residue was purified by column chromatography on silica gel (*n*-hexane/EtOAc = 8.5:1.5) to give V as colorless oils.

**General Procedure for the Preparation of Chromenes (VI).** V (0.01 mol) was dissolved in tetrahydrofuran (20 mL) and treated with 4 M hydrochloric acid (20 mL) for 4 h. The reaction mixture was subsequently extracted with methylene dichloride (3 × 20 mL). The combined organic layers were washed with 2 M aqueous sodium hydroxide solution (2 × 20 mL), ice/water (3 × 20 mL), and brine (2 × 20 mL) and were dried with anhydrous sodium sulfate. The solvent was evaporated in a vacuum. The residue was purified by column chromatography on silica gel (*n*-hexane/EtOAc = 9.75:0.25) to give VI as colorless oils.

**Candida albicans CYP51 Preparation and Enzyme Assay in Vitro.** CYP51 of *Candida albicans* ATCC 90028 (CYP51<sub>ATCC-1</sub>) was expressed in *Escherichia coli* JM-109 cells as described previously.<sup>30</sup> The CYP51 expressed in the membrane fraction of *E. coli* cells was purified after solubilization with sodium cholate. The detailed purification procedure will



be published elsewhere. The inhibitory activity of the lead compounds on fungal CYP51 was assayed in vitro with the purified *Candida albicans* CYP51<sub>ATCC-1</sub> preparation. CYP51-catalyzed lanosterol 14-demethylase activity was assayed with the reconstituted system consisting of the purified CYP51<sub>ATCC-1</sub> and purified *Saccharomyces cerevisiae* NADPH-P450 reductase. The reaction mixture containing 0.07 nmol of CYP51, 0.96 unit of NADPH-P450 reductase, 23.4 nmol of lanosterol (dispersed with dilauroylphosphatidylcholine), 0.1 mmol of potassium phosphate buffer, pH 7.2, and 1.0  $\mu$ mol of NADPH was made up to 1.0 mL. The lead compounds were added to the reaction mixture in 10  $\mu$ L of dimethyl sulfoxide solution. The reaction was started by the addition of NADPH and run aerobically at 30 °C for 5 min under constant shaking. The reaction was stopped by the addition of 2.5 mL of 10% KOH in methanol, and the mixture was saponified at 80 °C for 60 min. Then sterols were extracted with a mixture of diethyl ether and petroleum ether (5:95) and analyzed with gas-liquid chromatography as described previously.<sup>31</sup> The activity of CYP51 was calculated from the conversion ratio of lanosterol to the metabolite determined from the gas chromatograms.<sup>31</sup>

**Spectrophotometric Method.** Binding of the lead compounds to CYP51 was determined spectrophotometrically by the following procedure. The absorption spectrum of CYP51 (0.3  $\mu$ M) dissolved in 0.1 M potassium phosphate, pH 7.2, was recorded on a Shimadzu UV-2200 recording spectrophotometer. Then the same CYP51 solution was titrated successively with 10, 20, 40, 80, and 100  $\mu$ M of the lead compounds dissolved in DMSO. The absorption spectra observed in the presence of the lead compounds were recorded after each titration. The spectral changes of CYP51 caused by the addition of various concentrations of the compounds were obtained by subtracting the spectrum of free CYP51 from those recorded after the addition of the compounds.

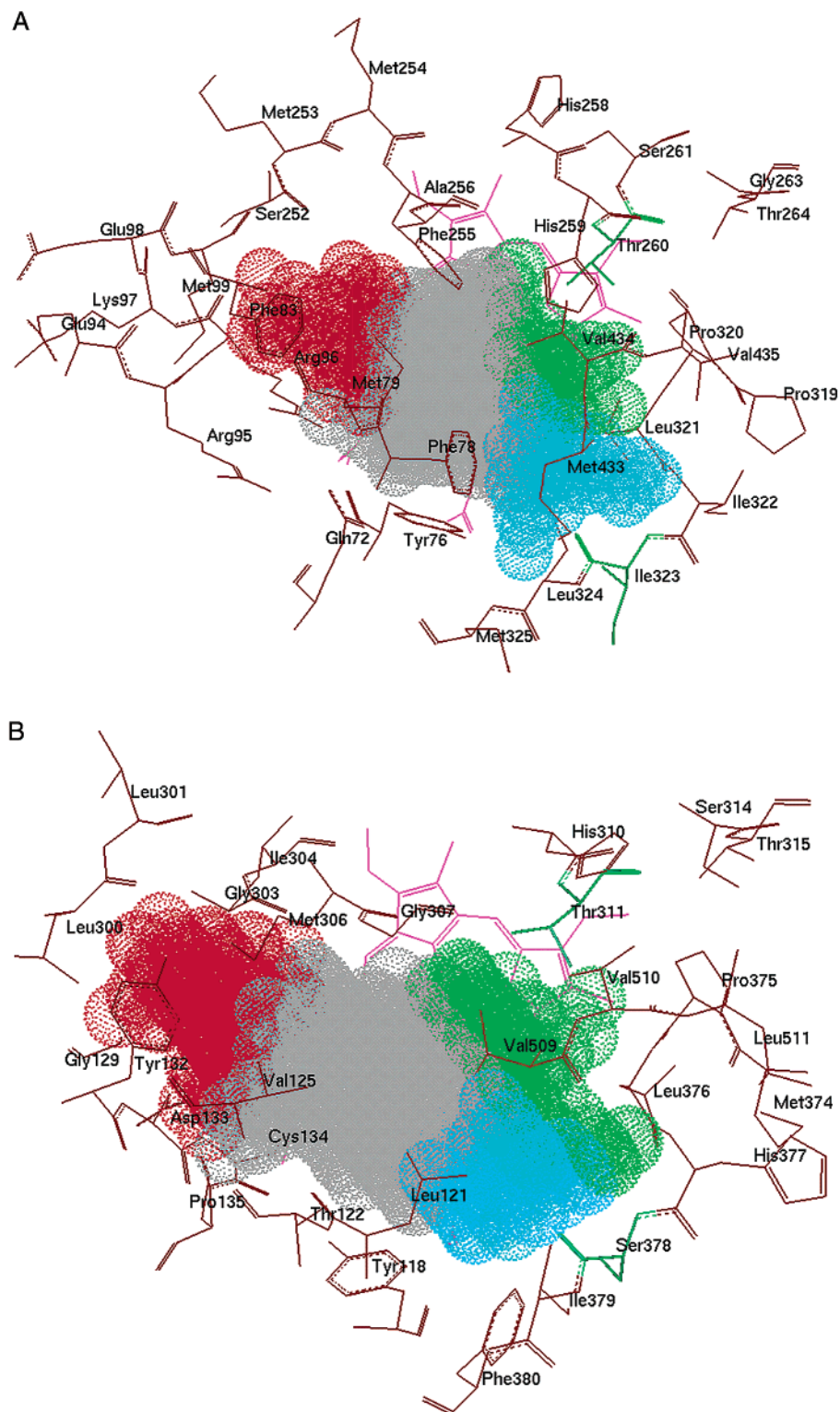
**In Vitro Antifungal Activity Assay.** In vitro antifungal activity was measured by means of the minimal inhibitory concentrations (MIC) using the serial dilution method in 96-well microtest plates. Test fungal strains were obtained from the ATCC or were clinical isolates. The MIC determination was performed according to the National Committee for Clinical Laboratory Standards (NCCLS) recommendations with RPMI 1640 (Sigma) buffered with 0.165 M MOPS (Sigma) as the test medium. The MIC value was defined as the lowest concentration of test compounds that resulted in a culture with turbidity less than or equal to 80% inhibition when compared with the growth of the control. Test compounds were dissolved in DMSO serially diluted in growth medium. The yeasts were incubated at 35 °C and the dermatophytes at 28 °C. Growth MIC was determined at 24 h for *Candida* species, at 72 h for *Cryptococcus neoformans*, and at 7 days for filamentous fungi.

## Results and Discussion

**1. Active Site of CYP51.** Prior to the design of an antifungal lead molecule, the active site of fungal CYP51 was investigated. Because the three-dimensional molecular model of CYP51 from *Candida albicans* was a theoretical structure constructed from the crystallographic coordinates of the four prokaryotic CYP51 enzymes, the active site of the crystal structure of the CYP51 from *Mycobacterium tuberculosis* was also investigated. We hope this crystal structure can afford some other useful information for inhibitor design. Just like the CYP51 from *Candida albicans*, the CYP51 from *Mycobacterium tuberculosis* can oxidize lanosterol, though the sequence identity between them is low (29%). All of the possible ligand binding cavities on the CYP51 were searched by the Binding Site Analysis program in InsightII. Four possible cavities in the crystal structure of CYP51 from *Mycobacterium tuberculosis* were found. The largest cavity (Figure 1A) with 614 grid points was the substrate-binding pocket, which is located in the

interior of the enzyme. The other three cavities were filled with 246, 148, and 137 grid points, respectively. These cavities were located on the protein surface, far away from the substrate-binding site. On the molecular model of CYP51 from *Candida albicans*, five possible cavities were identified. The largest cavity filled with 839 grid points was also the substrate-binding pocket, as shown in Figure 1B. The other four cavities with 348, 326, 302, and 249 grid points were located on the protein surface and also far away from the substrate-binding site. So the largest cavity involved in substrate binding and catalytic reaction was chosen as the active site for inhibitor design. The residues within 3 Å from any of the grid points defined in the largest cavity were indicated in Table 1. The shape and orientation of the active site of CYP51 from *Candida albicans* were similar to the shape and orientation from *Mycobacterium tuberculosis* (Figure 1). The bottom of the active site cavity was bound by the heme, and on the side, the active site cavity was bound by helix I, meander1,  $\beta$ 6-1/ $\beta$ 1-4, and  $\beta$ 6-2. Further outward from the heme were the C terminus of helix F, the  $\beta$ 1-5 N terminus of helix B', and the N terminus of helix A. Helix I,  $\beta$ 6-1/ $\beta$ 1-4, and  $\beta$ 6-2 were spatially conserved regions (SCRs) and played an important role in substrate catalysis and binding. The C terminus of helix F, the  $\beta$ 1-5 N-terminus of helix B', and the N terminus of helix A were spatially variable regions (SVRs). They composed the dome of the active site pocket and determined the size of the active site.<sup>32</sup>

The MCSS method was applied to explore the key regions in the active site that were essential for inhibitor binding. The nine aromatic, aliphatic, polar functional groups were mapped into the active site of CYP51 from *Mycobacterium tuberculosis* and from *Candida albicans* as summarized in Table 2. In general, except for the area in contact with the heme, both of the active sites can be divided into four subsites on the basis of the MCSS functionality mapping as shown in Figure 1. All of the low-energy minima of the ring functional groups such as hydrophobic benzene and cyclohexane or polar phenol were distributed over the hydrophobic S2 subsite, which was above the heme ring. The residues lining this subsite included the side chains of C376, V509, and V510 in *Candida albicans* or the side chains of L321, V434, and V435 in *Mycobacterium tuberculosis*. Many of the low-energy minima of alkyl functional groups (i.e., propane and butane) were also found to be distributed onto the S2 subsite. Others were found to be located in the S3 subsite. This subsite was a narrow and highly hydrophobic pocket formed by V125, C134, L300, and I304 in *Candida albicans* and by M79, F83, M99, L100, and A256 in *Mycobacterium tuberculosis*. The 17-alkyl side chain of the substrate lanosterol and the halogenated phenyl of azole inhibitors were also found to be located in this subsite, on the basis of the crystal structure and the docking analysis.<sup>18,19</sup> The polar groups methanol and ethanol were mainly scattered over the S1 and S4 subsites. The S1 subsite neighbored the central part of helix I, which was regarded as one of the few hydrophilic areas in the interior of cytochrome P450s.<sup>33</sup> Methanol and ethanol can form an H bond with the side chain hydroxyl group of the conserved threonine of helix I (T311 in *Candida albicans*, T260 in *Mycobac-*



**Figure 1.** Surface showing the active sites of CYP51 from *Mycobacterium tuberculosis* (A) and *Candida albicans* (B). Green indicates the S1 subsite. Gray indicates the S2 subsite. Red indicates the S3 subsite. Cyan indicates the S4 subsite.

*terium tuberculosis*). This residue had been found to be involved in the substrate catalytic reaction.<sup>34</sup> The S4 subsite was contiguous to the residues in the  $\beta 6$ -1/ $\beta 1$ -4 sheet. Methanol and ethanol can form hydrogen bonds with the backbone of the residues in the  $\beta 6$ -1/ $\beta 1$ -4 sheet, particularly the residue S378 in *Candida albicans* and the corresponding residue I323 in *Mycobacterium tuberculosis*. The ether minima were dispersed around most of the active site. In the S1 subsite, ether can form

hydrogen bonds with the side chain of the conserved histidine of helix I (H310 in *Candida albicans* and H259 in *Mycobacterium tuberculosis*). In the S4 subsite, ether can form hydrogen bonds with the backbone amino group of S378 in *Candida albicans* or I323 in *Mycobacterium tuberculosis*. The hydrophilic areas in the active site were explored by way of water MCSS calculation. Crystallographic solvent positions in the active site of CYP51 from *Mycobacterium tuberculosis* recurred. Most

**Table 1.** Active Site Residues of CYP51 within 3 Å from Any of the Grid Points Defined in the Largest Cavity

	<i>Mycobacterium tuberculosis</i>	<i>Candida albicans</i>
A helix, N terminus	F22, P26	Y69
β1-5-B' helix	Q72, Y76, F78, M79, F83	Y118, L121, T122, V125, G129
meander1	R96, M99, L100	I131, Y132, D133, C134, P135
F helix, C terminus	P178	L224, F228
I helix	S252, F255, A256, H259, T260	L300, G303, I304, M306, G307, Q309, H310, T311
β6-1 sheet	P320, L321, I322, I323, L324	L376, H377, S378, I379, F380
β6-2 sheet	H430, M433, V434, V435	S507, M508, V509, V510, L511

**Table 2.** Functional Groups Used in the MCSS Calculation

MCSS functional groups	initial no. of copies	no. of minima	range of $U_{\text{bind}}^a$ for minima (kcal/mol)		selected minima in lead design (kcal/mol)
			from	to	
<i>Mycobacterium tuberculosis</i>					
benzene	5000	15	-9.57	-20.21	
cyclohexane	5000	65	-1.40	-9.68	
propane	5000	67	-4.17	-7.13	
butane	5000	180	-0.37	-8.46	
phenol	5000	71	-6.66	-31.82	
methanol	5000	47	-5.04	-29.19	
ether	5000	27	-0.89	-18.55	
ethanol	5000	144	-0.02	-29.33	
water	5000	34	-2.93	-32.08	
<i>Candida albicans</i>					
benzene	5000	32	-6.91	-13.51	no. 2: -13.16
cyclohexane	5000	66	-0.11	-9.41	no. 1: -9.41
propane	5000	76	-4.11	-7.71	no. 1: -7.71
butane	5000	200	-2.16	-9.08	no. 1: -9.08
phenol	5000	198	-5.75	-17.52	no. 1: -17.52 no. 11: -16.14
methanol	5000	79	-0.77	-15.55	no. 1: -15.55 no. 20: -10.59
ether	5000	48	-4.21	-10.54	no. 10: -9.35
ethanol	5000	252	-0.29	-15.55	no. 1: -15.55 no. 59: -11.22
water	5000	55	-1.93	-20.54	no. 1: -20.54 no. 5: -13.93

<sup>a</sup>  $U_{\text{bind}}$ , the binding energy for a given functional group in each minimized replica obtained from the MCSS calculation, was defined as  $U_{\text{bind}} = U_{\text{protein-group}} + U_{\text{group}} - U_{\text{group}}^0$ , where  $U_{\text{protein-group}}$  represents the nonbonded interactions between the CYP51 and the given functional group,  $U_{\text{group}}$  represents the internal energy of the functional group within the complex, and  $U_{\text{group}}^0$  represents the internal energy of the isolated functional group in a vacuum, respectively.

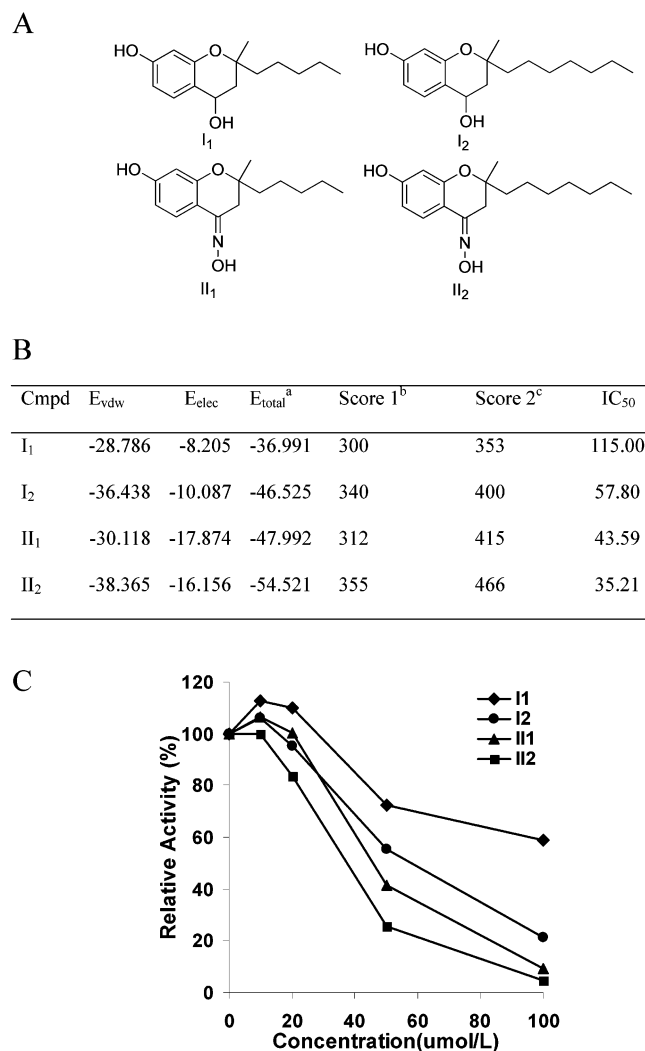
of the water minima were located in the S1 subsite. Some minima were also found to form hydrogen bonds with the backbone of S378 in *Candida albicans* and I323 in *Mycobacterium tuberculosis*. The important regions in the active site for ligand binding were further explored by the LUDI program. LUDI is a knowledge-based ligand design program with a set of geometric rules derived from a statistical analysis of a series of ligand-receptor crystal structures. The S1 subsite was the hydrogen bond donor region. The S2 and S3 subsites were the hydrophobic regions, and the S4 subsite was the hydrogen bond donor and acceptor region.

**2. Lead Structure Design and Inhibitory Effect on CYP51 from *Candida albicans*.** Except for the site coordinating with the heme, the key regions in the active site of CYP51 for ligand noncovalent binding can be divided into four subsites by the investigation of the three-dimensional molecular model of CYP51 from *Candida albicans* and the crystal structure of CYP51 from *Mycobacterium tuberculosis*. The S1 subsite was the hydrophilic hydrogen-bonding region. The catalyti-

cally essential threonine (T311 in *Candida albicans*) can act as an important candidate to form a hydrogen bond with ligands. The S2 subsite was the hydrophobic region. Most of the three phenyl rings of clotrimazole were located in this area. The S3 subsite was the narrow hydrophobic cleft formed by the residues in the helix B'-meander1 loop and the N terminus of helix I. The 17-alkyl side chain of lanosterol is supposed to be located in this area.<sup>18</sup> The S4 subsite adjacent to the β6-1/β1-4 sheet is another important hydrogen-bonding region in the active site. The 3-hydroxyl group of lanosterol has been supposed to form hydrogen bonds with residue S378 in the β6-1/β1-4 sheet of *Candida albicans*.<sup>18,35</sup> In the crystal structure of CYP51 from *Mycobacterium tuberculosis* in complex with fluconazole, the N-3 atom of theazole ring that did not coordinate with the heme is found to form an H bond with the backbone carbonyl group of I323 in the β6-1/β1-4 sheet through the bridging of a structural water.

In the MCSS calculation for the active site of CYP51 from *Candida albicans*, the minima with the most favorable interaction energies for the polar functional groups such as methanol (minimum no. 1, -15.55 kcal/mol), ethanol (minimum no. 1, -15.55 kcal/mol), phenol (minimum no. 1, -17.52 kcal/mol), and water (minimum no. 1, -20.54 kcal/mol) were located in the S4 subsite and formed hydrogen bonds with the backbone carbonyl group of residue S378, as listed in Table 2. Minimum no. 20 (-10.59 kcal/mol) for methanol, minimum no. 59 (-11.22 kcal/mol) for ethanol, minimum no. 11 (-16.14 kcal/mol) for phenol, and minimum no. 5 (-13.93 kcal/mol) for water were located in the S1 subsite and were involved in hydrogen-bonding interactions with the side chain hydroxyl group of residue T311. The minima displaying the most favorable interaction energies for the ring lipophilic group (i.e., minimum no. 1 is -9.41 kcal/mol for cyclohexane and is -13.16 kcal/mol for benzene) were located in the S2 subsite. The phenyl ring moieties of phenol minimum nos. 1 and 11 were also located in the S2 subsite. The minima with the most favorable interaction energies for the alkyl lipophilic functional groups (i.e., minimum no. 1 is -7.71 kcal/mol for propane and is -9.08 kcal/mol for butane) were located in the S3 subsite. Because the polar ether functional group is somewhat lipophilic, minimum no. 10 (-9.35 kcal/mol) was located in the S2 subsite. By connecting the highest scoring minimum of the above functional groups in each subsite, several different types of lead structures were designed. Figure 2A shows some of the designed lead molecules containing the benzopyran ring. At position 2 of the lead structure, long lipophilic alkyl side chains were introduced to interact with the hydrophobic S3 subsite. The 7-phenolic hydroxyl group was chosen to form an H bond with the side chain hydroxyl group of the catalytic residue T311





**Figure 2.** (A) Chemical structure of the designed lead compounds. (B) Calculated interaction energies (kcal/mol) for the complexes of the lead compounds with the active site of CYP51 of *Candida albicans*, Ludi scores, and experimentally determined binding affinity (IC<sub>50</sub>, μmol/L) of the lead compound for the reconstituted CYP51 from *Candida albicans*. Footnote a:  $E_{total} = E_{vdw} + E_{elec}$ . Footnote b: for score 1, the LUDI score was calculated by the method in ref 28. Footnote c: for score 2, the LUDI score was calculated by the method in ref 29. (C) Inhibition of the activity of CYP51 from *Candida albicans* by lead compounds. The activity of CYP51 was assayed as described in Materials and Methods in the presence of the indicated concentration of lead compounds I<sub>1</sub> (◆), I<sub>2</sub> (●), II<sub>1</sub> (▲), and II<sub>2</sub> (■).

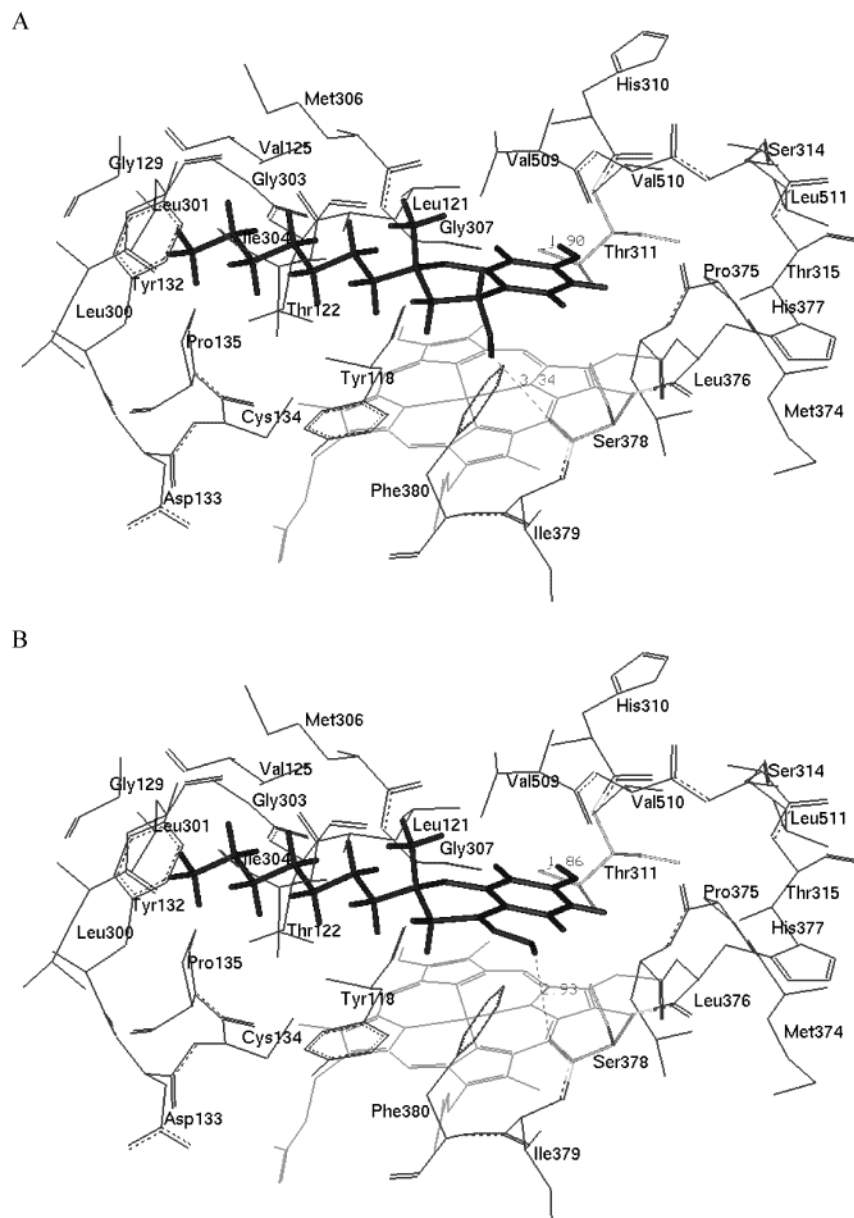
in the S1 subsite. 4-Hydroxyl and 4-hydroxyimino groups were introduced to form hydrogen-bonding interactions with the backbone carbonyl group of S378 in the S4 subsite. In the S2 subsite, the benzopyran ring was selected to act as the skeleton to link the functional groups in the S1, S2, and S3 subsites and also because of the synthetic accessibility. In addition, the methyl group was introduced at position 2 of the benzopyran ring to form an excellent complementary contact with the side chain methyl groups of L121 and V125. After energy minimization, the lowest energy position in the active site for the generated lead molecule was determined by the flexible ligand docking procedure in the Affinity module of the InsightII program. The calculated interaction energies and LUDI scores of each molecule

are given in Figure 2B, with IC<sub>50</sub> values for in vitro inhibition of CYP51 from *Candida albicans*. The overall trend for the interaction energy and LUDI scores are in good qualitative agreement with the experimental data.

The mode of action of lead molecules I<sub>1</sub> and II<sub>1</sub> with the active site of CYP51 *Candida albicans* is shown in parts A and B of Figure 3, respectively. After flexible ligand docking and subsequent molecular dynamics simulated annealing studies, the 4-hydroxyl group of I<sub>1</sub>, which was initially introduced to form an H bond with the backbone carbonyl oxygen atom of residue S378, moved away and was closer to the heme iron atom to give the total system the lowest energy. The distance between the hydrogen atom of the 4-hydroxyl group of I<sub>1</sub> and the carbonyl oxygen atom of residue S378 was 3.34 Å, which is difficult for forming a hydrogen bond, as shown in Figure 3A. For II<sub>1</sub>, the situation was different. The 4-hydroxyimino group of II<sub>1</sub> is conjugated with the phenyl ring, and the distance between the hydrogen atom of the 4-hydroxyimino group and the carbonyl oxygen atom of residue S378 is 2.93 Å. They can form a hydrogen-bonding interaction as indicated in Figure 3B.

Figure 2C shows the inhibitory effects of lead compounds I<sub>1</sub>, I<sub>2</sub>, II<sub>1</sub>, and II<sub>2</sub> on the lanosterol 14 $\alpha$ -demethylase activity of the reconstituted system consisting of purified CYP51 from *Candida albicans* and NADPH-P450 reductase purified from *Saccharomyces cerevisiae*. All of the lead compounds strongly inhibit the demethylase. The inhibition is linearly dependent on their concentrations. Compound II<sub>2</sub> is the most potent inhibitor of CYP51 from *Candida albicans*, and its IC<sub>50</sub> value is 35.21 μmol/L. The inhibitory effects of compounds II<sub>1</sub> and II<sub>2</sub> are stronger than those of I<sub>1</sub> and I<sub>2</sub>, respectively, indicating that the 4-hydroxyimino group is more favorable for the inhibition of the reconstituted enzyme system than the 4-hydroxyl group. The inhibitory effects of compounds I<sub>2</sub> and II<sub>2</sub> are stronger than those of I<sub>1</sub> and II<sub>1</sub>, respectively, suggesting that the compound with the longer alkyl side chain makes close contact with the hydrophobic S3 subsite in the active site. From comparisons with the inhibitory effects of compounds I<sub>1</sub>, II<sub>1</sub>, and I<sub>2</sub>, we found that the insertion of an imino group into the C–O bond at position 4 plays a more important role in the inhibitor binding than the introduction of two carbon atoms at the terminus of the 2-alkyl side chain. All of the compounds except II<sub>2</sub> exhibited a weak capability of accelerating the conversion of the substrate lanosterol into its metabolite at a low concentration (Figure 2C). However, the mechanism of action was not known until now.

**3. Derivative Design and Structure–Activity Relationships.** Some derivatives of the lead compounds were subsequently designed to investigate the mode of action of the lead inhibitors with the active site of CYP51. The lead inhibitors and their derivatives were prepared as shown in Schemes 1 and 2. 4-Chromanones (III) were synthesized by the reaction of 2,4-dihydroxyacetophenone with alkyl methyl ketones in the presence of pyrrolidine. The yield was improved using ethanol as the solvent and molecular sieves as a water trap. The lead compound 4,7-chromanediols (I<sub>1</sub>–I<sub>3</sub>) were synthesized using LiAlH<sub>4</sub> to reduce III. The lead compound



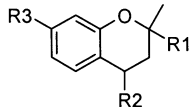
**Figure 3.** Binding of lead compounds **I**<sub>1</sub> and **II**<sub>1</sub> to the active site of CYP51 from *Candida albicans*. The distances between the specific hydrogen bond donor of lead compounds (hydrogen atom of the 7-phenolic hydroxyl group, hydrogen atom of the 4-hydroxyl group, or hydrogen atom of the 4-hydroxylimino group) and the specific hydrogen bond acceptor in the active site (oxygen atom of side chain hydroxyl group of A311 or oxygen atom of backbone carbonyl group of A378) are indicated.

4,7-oximinochromanes (**III**<sub>1</sub>–**III**<sub>3</sub>) were obtained by the reaction of 4-chromanones (**III**) with hydroxylamine in ethanol. Treatment of **III** with CH<sub>3</sub>I in the presence of K<sub>2</sub>CO<sub>3</sub>/acetone gave the O-alkylated derivatives (**IV**). Reduction of **IV** with NaBH<sub>4</sub> provided 4-chromanol derivatives (**V**). **V** was then converted to chromenes (**VI**) by treatment with 4 M HCl. Each of the title compounds was confirmed by <sup>1</sup>H NMR, elemental analysis, IR spectrum, and mass spectrum. Some were further confirmed by <sup>13</sup>C NMR and high-resolution mass spectra (the physical data for the compounds are given in the table in Supporting Information).

The results of in vitro antifungal activities of the title compounds are listed Table 3. All of the lead molecules exhibited antifungal activities against eight pathogenic fungi, and compounds **II**<sub>2</sub> exhibited the highest activity, indicating that the lead compounds can inhibit not only the metabolism of the substrate lanosterol but also the

growth of fungal cells. The antifungal activities of the 4-oxo analogues, compounds **III**<sub>1</sub>, **III**<sub>2</sub>, and **III**<sub>3</sub>, are lower than those of the lead inhibitors (**I**, **II**), suggesting that the appropriate substitution at position 4 of the compound is important for antifungal activities. As mentioned above, the S3 subsite is the narrow hydrophobic cleft formed by the residues in the helix B'–meander1 loop and the N terminus of helix I, which is supposed to bind the 17-alkyl side chain of the substrate. Since the size of this cavity is limited by the molecular model, analogues with different lengths of the 2-alkyl side chains were designed to verify the molecular model and also to analyze the relationship between the length of alkyl side chain and their antifungal activity. Compared to **III**<sub>1</sub>, **III**<sub>2</sub>, and **III**<sub>3</sub>, compound **III**<sub>4</sub> exhibited no antifungal activity. It is because the alkyl side chain of **III**<sub>4</sub> is too long to be accommodated by the hydrophobic S3 subsite. **III**<sub>5</sub> is less potent than **III**<sub>1</sub>–



**Table 3.** Derivatives Design and Antifungal in Vitro Activities (MIC,  $\mu\text{g/mL}$ )<sup>a</sup>


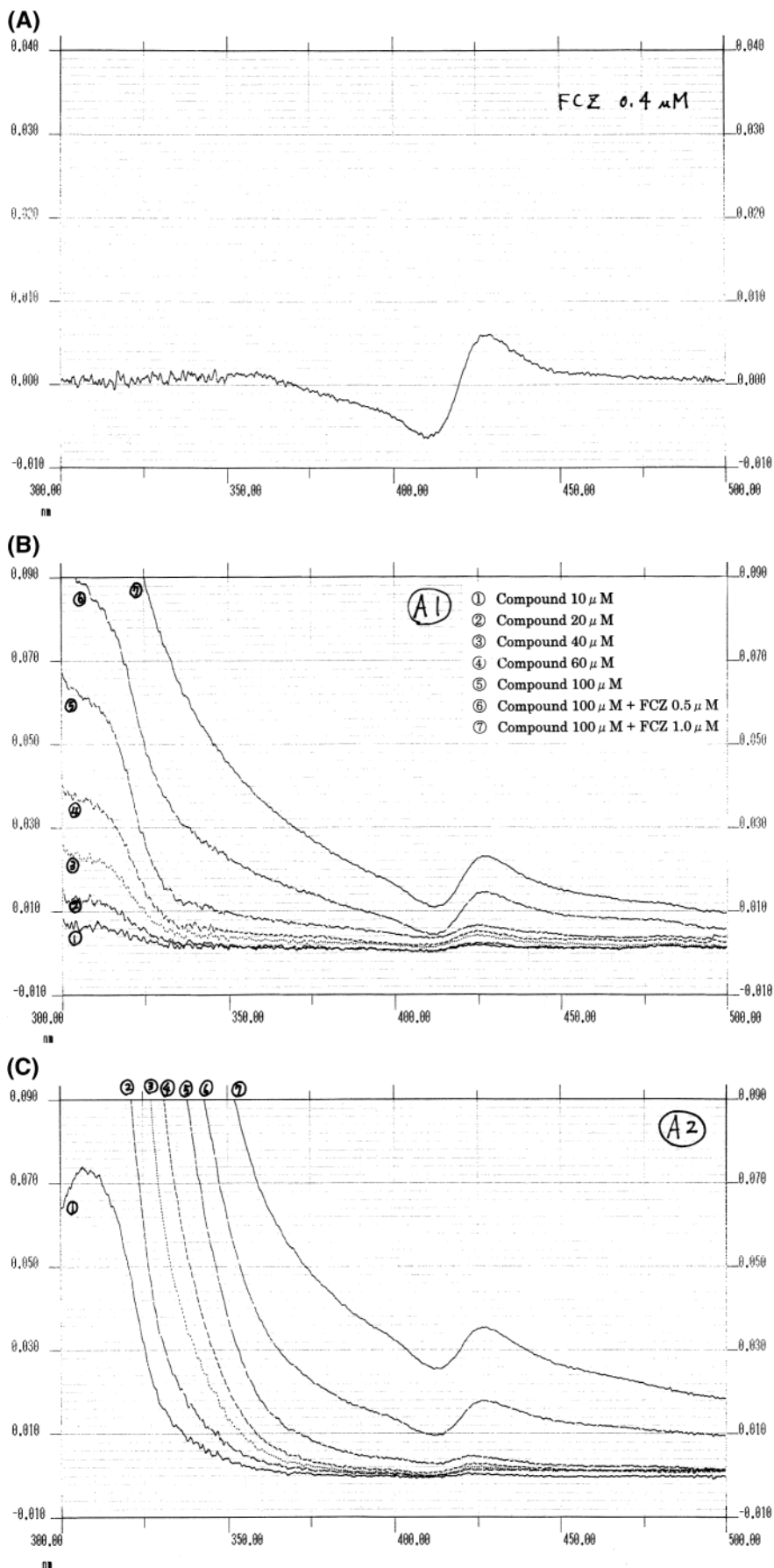
compd	R <sub>1</sub>	R <sub>2</sub>	R <sub>3</sub>	MIC, $\mu\text{g/mL}$							
				<i>C. alb.</i>	<i>C. par.</i>	<i>C. neo.</i>	<i>S. sch.</i>	<i>F. ped.</i>	<i>A. fum.</i>	<i>T. rub.</i>	<i>M. can.</i>
<b>I<sub>1</sub></b>	CH <sub>2</sub> (CH <sub>2</sub> ) <sub>3</sub> CH <sub>3</sub>	OH	7-OH	160	40	80	20	40	80	20	10
<b>I<sub>2</sub></b>	CH <sub>2</sub> (CH <sub>2</sub> ) <sub>5</sub> CH <sub>3</sub>	OH	7-OH	40	20	40	40	80	80	20	2.5
<b>I<sub>3</sub></b>	CH <sub>2</sub> CH <sub>2</sub> CH=C(CH <sub>3</sub> ) <sub>2</sub>	OH	7-OH	80	80	160	80	160	160	80	10
<b>II<sub>1</sub></b>	CH <sub>2</sub> (CH <sub>2</sub> ) <sub>3</sub> CH <sub>3</sub>	=NOH	7-OH	160	40	40	40	40	80	5	5
<b>II<sub>2</sub></b>	CH <sub>2</sub> (CH <sub>2</sub> ) <sub>5</sub> CH <sub>3</sub>	=NOH	7-OH	40	20	20	10	40	10	2.5	0.625
<b>II<sub>3</sub></b>	CH <sub>2</sub> CH <sub>2</sub> CH=C(CH <sub>3</sub> ) <sub>2</sub>	=NOH	7-OH	80	40	40	40	20	40	5	2.5
<b>III<sub>1</sub></b>	CH <sub>2</sub> (CH <sub>2</sub> ) <sub>3</sub> CH <sub>3</sub>	=O	7-OH	320	160	160	80	80	160	20	40
<b>III<sub>2</sub></b>	CH <sub>2</sub> (CH <sub>2</sub> ) <sub>5</sub> CH <sub>3</sub>	=O	7-OH	160	160	80	40	80	160	40	80
<b>III<sub>3</sub></b>	CH <sub>2</sub> CH <sub>2</sub> CH=C(CH <sub>3</sub> ) <sub>2</sub>	=O	7-OH	160	80	160	160	160	80	80	40
<b>III<sub>4</sub></b>	CH <sub>2</sub> (CH <sub>2</sub> ) <sub>7</sub> CH <sub>3</sub>	=O	7-OH	>320	>320	>320	>320	>320	80	>320	80
<b>III<sub>5</sub></b>	CH <sub>2</sub> CH(CH <sub>3</sub> ) <sub>2</sub>	=O	7-OH	>320	320	320	320	160	160	160	40
<b>IV<sub>1</sub></b>	CH <sub>2</sub> (CH <sub>2</sub> ) <sub>3</sub> CH <sub>3</sub>	=O	7-OCH <sub>3</sub>	>320	>320	>320	>320	>320	160	>320	80
<b>IV<sub>2</sub></b>	CH <sub>2</sub> (CH <sub>2</sub> ) <sub>5</sub> CH <sub>3</sub>	=O	7-OCH <sub>3</sub>	>320	320	>320	40	>320	>320	320	40
<b>IV<sub>3</sub></b>	CH <sub>2</sub> CH <sub>2</sub> CH=C(CH <sub>3</sub> ) <sub>2</sub>	=O	7-OCH <sub>3</sub>	>320	>320	>320	320	>320	160	>320	80
<b>V<sub>1</sub></b>	CH <sub>2</sub> (CH <sub>2</sub> ) <sub>3</sub> CH <sub>3</sub>	OH	7-OCH <sub>3</sub>	320	160	160	>320	>320	80	20	20
<b>V<sub>2</sub></b>	CH <sub>2</sub> (CH <sub>2</sub> ) <sub>5</sub> CH <sub>3</sub>	OH	7-OCH <sub>3</sub>	320	160	80	40	160	80	80	80
<b>V<sub>3</sub></b>	CH <sub>2</sub> CH <sub>2</sub> CH=C(CH <sub>3</sub> ) <sub>2</sub>	OH	7-OCH <sub>3</sub>	>320	160	160	320	320	160	160	160
<b>VI<sub>1</sub></b>	CH <sub>2</sub> (CH <sub>2</sub> ) <sub>3</sub> CH <sub>3</sub>	$\Delta^{3,4}$	7-OCH <sub>3</sub>	>320	>320	320	>320	>320	>320	>320	320
<b>VI<sub>2</sub></b>	CH <sub>2</sub> (CH <sub>2</sub> ) <sub>5</sub> CH <sub>3</sub>	$\Delta^{3,4}$	7-OCH <sub>3</sub>	>320	>320	>320	>320	>320	>320	>320	320
<b>VI<sub>3</sub></b>	CH <sub>2</sub> CH <sub>2</sub> CH=C(CH <sub>3</sub> ) <sub>2</sub>	$\Delta^{3,4}$	7-OCH <sub>3</sub>	>320	>320	>320	320	>320	>320	40	80
	fluconazole			4	8	32	0.25	64	16	0.5	0.5

<sup>a</sup> Abbreviations: *C. alb.*, *Candida albicans*; *C. par.*, *Candida parapsilosis*; *C. neo.*, *Cryptococcus neoformans*; *S. sch.*, *Sporothrix schenckii*; *F. ped.*, *Fonsecaea pedrosoi*; *A. fum.*, *Aspergillus fumigatus*; *T. rub.*, *Trichophyton rubrum*; *M. can.*, *Microsporium canis*.

**III<sub>3</sub>** because its alkyl side chain is too short to interact firmly with the hydrophobic region, although it is able to enter the active site. All of these findings suggest that the size of the hydrophobic pocket in the active site is limited. The alkyl side chains with four to seven carbon atoms are favorable for antifungal activity. To study whether the 7-hydroxyl group of the lead inhibitors formed an H-bond with the hydroxyl group of the side chain of residue T311 in the hydrophilic hydrogen-bonding pocket, we designed the hydrophobic 7-methoxyl analogues and observed the changes in antifungal activity. When the 7-hydroxyl groups of **III<sub>1</sub>**, **III<sub>2</sub>**, and **III<sub>3</sub>** are changed into 7-methoxyl groups, the antifungal activities of the compounds **IV<sub>1</sub>**–**IV<sub>3</sub>** decrease dramatically. It is suggested that the corresponding binding region in the active site is a hydrophilic pocket and that the hydrogen bond between the side chain hydroxyl group of residue T311 and the 7-hydroxyl group of the inhibitors is broken. When the 4-carbonyl groups of **IV<sub>1</sub>**–**IV<sub>3</sub>** are reduced to 4-hydroxyl groups (compounds **V<sub>1</sub>**–**V<sub>3</sub>**), the antifungal activities of the resulting analogues increase again, showing that polar substituents at position 4 are more favorable. When the 4-hydroxyl groups of compounds **V<sub>1</sub>**–**V<sub>3</sub>** are converted into 2H-1-chromene derivatives (**VI<sub>1</sub>**–**VI<sub>3</sub>**), the antifungal activities disappear again. In short, the SAR analysis here shows that the 2-hydrophobic side chain, the 4-hydrogen bond donor/acceptor, and the 7-hydrophilic hydrogen bond donor of the lead inhibitors are the determinants for antifungal activities, which are also in accordance with the molecular model. Compared to fluconazole, the lead inhibitors and their derivatives exhibited a lower antifungal activity, which might be caused by the following two factors. First, the inhibitors reported in this study were obtained by linking the molecular fragments that were used in the MCSS calculation. These molecular fragments are usually employed to

probe the distribution of molecular interaction fields (MIFs) in the active site, but not the optimal functional groups interacting with a specific active site. Second, the receptor used in this study was modeled on the basis of the coordinates of the prokaryotic enzymes, and the sequence identity between them is rather low. The uncertain atom coordinates of the residues are also an important determinant that limits the development of high potent inhibitors.

**4. Spectrophotometric Analyses of the Interaction of Lead Compounds with Ferric CYP51.** Binding of the lead compounds to ferric CYP51 was analyzed spectrophotometrically. Figure 4A represents a typical type II difference spectrum induced by the azole ring of fluconazole. Parts B and C of Figure 4 show the spectral changes of ferric CYP51 induced by lead compounds **I<sub>1</sub>** and **II<sub>1</sub>**, respectively. Because the lead compounds do not have a nitrogen atom that can coordinate to the heme iron atom of CYP51, their spectra are quite different from that of fluconazole. However, the small but clear spectral changes caused by the addition of **I<sub>1</sub>** or **II<sub>1</sub>** alone are characteristic of a type II difference spectrum (spectra 1–5 of parts B and C of Figure 4),<sup>36</sup> which is due to the interaction between one of the two hydroxyl groups of the lead compounds and the heme iron atom. The intensity of the difference spectra caused by the addition of **I<sub>1</sub>** was larger than that caused by **II<sub>1</sub>**, suggesting that the red shift of the Soret peak induced by **I<sub>1</sub>** is larger than that caused by **II<sub>1</sub>**. The extent of the red shift of the Soret peak is dependent on the ligand-field strength of the ligand atom that interacts with the heme iron atom. The ligand-field strength of the ligand atom is determined by the electronegativity of the coordinating atom and the distance and angle of the coordinating bond. Both **I<sub>1</sub>** and **II<sub>1</sub>** have 7-phenolic hydroxyl groups. If the 7-phenolic hydroxyl group had acted as the external sixth ligand, the electronegativity



**Figure 4.** Spectral changes of ferric CYP51 caused by binding of azole antifungal agents and the lead compounds: (A) fluconazole-induced difference spectrum; (B) difference spectra induced by I<sub>1</sub> alone (spectra 1–5) and by the combined addition of I<sub>1</sub> and fluconazole (spectra 6 and 7); (C) difference spectra induced by II<sub>1</sub> alone (spectra 1–5) and by the combined addition of II<sub>1</sub> and fluconazole (spectra 6 and 7).

of the hydroxyl group and the distance and (or) the bond angle of the coordinating bond should have been different. The structural feature in the vicinity of the 7-phenolic hydroxyl group of **I**<sub>1</sub> is identical with that of **II**<sub>1</sub>, suggesting that the distance and bond angle of the coordinating bond should be the same. This suggests that the electronegativity of the 7-phenolic hydroxyl oxygens should be different.

The conformation space of compounds **I**<sub>1</sub> and **II**<sub>1</sub> was explored by molecular dynamics simulated annealing and the systematic conformational search method. The obtained lowest energy conformation was then selected as the initial conformation to perform full geometry optimization using an ab initio calculation method at the HF/6-31G, B3LYP/6-31G, and B3LYP/6-31G(d) levels sequentially. The global minimum energy conformation was obtained, and the vibrational frequency was derived. No imaginary frequencies existed for both molecules, suggesting that the structures correspond to a real minimum on the potential energy surface. The electron properties of the global minimum energy conformation were calculated by the B3LYP/6-31G(d) method. The partial charge of the 7-phenolic hydroxyl group in **I**<sub>1</sub> ( $Q_o = -0.646$ ) was almost identical to that of **II**<sub>1</sub> ( $Q_o = -0.642$ ), indicating that the 7-phenolic hydroxyl group is not the candidate interacting with the iron atom of heme.

The partial charge of the oxygen atom of the 4-hydroxyl group in **I**<sub>1</sub> ( $Q_o = -0.625$ ) was very different from that of the 4-hydroxylimino group in **II**<sub>1</sub> ( $Q_o = -0.510$ ), and the oxygen atom of the 4-hydroxyl group in **I**<sub>1</sub> had more negative charge. From the molecular models of the active site in complex with the lead molecules (Figure 3), the benzopyran ring was located in the hydrophobic S2 subsite, which was above the heme iron atom. All of these findings suggested that the 4-hydroxyl group of **I**<sub>1</sub> and the 4-hydroxylimino group of **II**<sub>1</sub> are the most reasonable candidates for interacting with the heme iron atom, and the oxygen atom of the 4-hydroxyl group of **I**<sub>1</sub> forms a stronger interaction with the heme iron atom than the oxygen atom of the 4-hydroxylimino group of **II**<sub>1</sub>.

However, it is very interesting that the inhibitory effect of compound **II**<sub>1</sub> is stronger than that of **I**<sub>1</sub>. Both compounds have the same chemical structure except for the substituent at position 4. If the 4-hydroxyl group of **I**<sub>1</sub> and the 4-hydroxylimino group of **II**<sub>1</sub> had interacted with the heme iron atom, the inhibitory effect of **I**<sub>1</sub> should have been stronger than that of **II**<sub>1</sub> because the oxygen atom of the 4-hydroxyl group of **I**<sub>1</sub> forms a stronger interaction with the heme iron atom than the oxygen atom of the 4-hydroxylimino group of **II**<sub>1</sub>. From the molecular model, the 4-hydroxyl group of **I**<sub>1</sub>, which is attached to an sp<sup>3</sup>-hybridized carbon atom, deviates from the phenyl ring and is closer to the heme iron atom after flexible ligand docking and energy minimization as described above (Figure 3A), while the 4-hydroxylimino group of **II**<sub>1</sub> is coplanar with the phenyl ring and a little farther away from the heme iron atom (Figure 3B). The appropriate distance and spatial orientation encouraged the formation of a weak hydrogen bond between the hydrogen atom of the 4-hydroxylimino group of **II**<sub>1</sub> and the backbone carbonyl oxygen atom of residue S378. This may be the explanation for the

phenomenon that the intensity of the difference spectrum caused by **I**<sub>1</sub> is larger than that caused by **II**<sub>1</sub> while the inhibitory effect of compound **I**<sub>1</sub> is lower than that of **II**<sub>1</sub>. We suppose it is possible that other functional groups coplanar with the phenyl ring moiety could be introduced at position 4 to form strong hydrogen bonds with the backbone of S378 but not interacting with the heme iron atom. The interaction between the oxygen atom of lead compounds and the heme iron atom was rather low because the intensity of the type II difference spectra of the lead compound was much smaller than that ofazole antifungal agents such as fluconazole. Therefore, the affinity of the lead compounds for CYP51 is mainly attributed to their nonbonded interaction with the apoprotein, which affords the opportunity to develop novel non-azole antifungal agents without the cross inhibition of other cytochrome P450 proteins due to the coordination binding with the heme iron atom.<sup>9</sup>

It is also noteworthy that the difference spectra induced by the combined addition of the lead compounds and fluconazole (spectra 6 and 7 of parts B and C of Figure 4) are apparently smaller than the difference spectrum induced by fluconazole alone (Figure 4A). This fact suggests that the lead compound partially interferes with the binding of fluconazole in a competitive manner. The difference spectrum induced by the combined addition of compound **II**<sub>1</sub> and fluconazole is smaller than the difference spectrum induced by the combined addition of compound **I**<sub>1</sub> and fluconazole, indicating that compound **II**<sub>1</sub> is a stronger competitive inhibitor.

## Conclusion

Starting with the three-dimensional molecular model of CYP51 from *Candida albicans* and the crystal structure of CYP51 from *Mycobacterium tuberculosis*, a structure-based de novo ligand design strategy was utilized to search for an antifungal lead inhibitor. Except for the site coordinating with the heme, the key regions in the active site for noncovalent ligand binding can be divided into four subsites after MCSS functional group mapping and LUDI calculation. The S1 subsite is the hydrophilic hydrogen-bonding region. The S2 and S3 subsites are the hydrophobic regions. The S4 subsite adjacent to the  $\beta_6-1/\beta_1-4$  sheet was another important hydrogen-bonding region in the active site. Several non-azole lead molecules were designed to interact with the above four subsites. All of the lead molecules exhibited a strong inhibitory effect on lanosterol 14 $\alpha$ -demethylase from *Candida albicans*, and compound **B2** was the most potent inhibitor. They occupy the substrate-binding site and interfere with the binding ofazole antifungal agents. The interactions between the lead molecules and the active site of CYP51 were validated by spectrophotometric analysis and derivatives design. This is the first successful example reported for the inhibitor design of the cytochrome P450 superfamily using the de novo design strategy. The studies presented here provide a pathway to design novel antifungal compounds that do not coordinate to the heme iron atom. On the other hand, the biological activity of the lead compounds is mainly attributed to their nonbonded interaction with the apoprotein of CYP51, which affords an opportunity to develop novel antifungal agents specific for the fungal enzyme but without the serious toxicity due to cross



inhibition of other cytochrome P450 proteins. In addition, it should be pointed out that all of the lead molecules were designed on the basis of a homology-derived molecular model of CYP51 from *Candida albicans*. The de novo ligand design approach based on a homology model established in this study should have general implications for searching novel inhibitors of other membrane-binding enzymes.

**Acknowledgment.** The work was supported in part by the National Natural Science Foundation of China (Grant Nos. 39770876 and 39470830).

**Supporting Information Available:** Structural data for the compounds in this study. This material is available free of charge via the Internet at <http://pubs.acs.org>.

## References

- Vanden Bossche, H.; Koymans, L. Cytochrome P450 in fungi. *Mycoses* **1998**, *41*, 32–38.
- Yoshida, Y.; Aoyama, Y.; Noshiro, M.; Gotoh, O. Sterol 14-demethylase P450 (CYP51) provides a breakthrough for the discussion on the evolution of cytochrome P450 gene family. *Biochem. Biophys. Res. Commun.* **2000**, *273*, 799–804.
- Kelly, S. L.; Lamb, D. C.; Cannieux, M.; Greetham, D.; Jackson, C. J.; Marczylo, T.; Ugochukwu, C.; Kelly, D. E. An old activity in the cytochrome P450 superfamily (CYP51) and a new story of drugs and resistance. *Biochem. Soc. Trans.* **2001**, *29*, 122–128.
- Sheehan, D. J.; Hitchcock, C. A.; Sibley, C. M. Current and emerging azole antifungal agents. *Clin. Microbiol. Rev.* **1999**, *12*, 40–79.
- Georgopadakou, N. H.; Walsh, T. J. Antifungal agents: chemotherapeutic targets and immunologic strategies. *Antimicrob. Agents Chemother.* **1996**, *40*, 279–291.
- Lupetti, A.; Danesi, R.; Campa, M.; Tacca, M. D.; Kelly, S. Molecular basis of resistance to azole antifungals. *Trends Mol. Med.* **2002**, *8*, 76–81.
- Lamb, D. C.; Kelly, D. E.; Baldwin, B. C.; Kelly, S. L. Differential inhibition of human CYP3A4 and *Candida albicans* CYP51 with azole antifungal agents. *Chem. Biol. Interact.* **2000**, *125*, 165–175.
- Slama, J. T.; Hancock, J. L.; Rho, T.; Sambucetti, L.; Bachmann, K. A. Influence of some novel N-substituted azole and pyridines on rat hepatic CYP3A activity. *Biochem. Pharmacol.* **1998**, *55*, 1881–1892.
- Wulff, H.; Miller, M. J.; Hänsel, W.; Grissmer, S.; Cahalan, M. D.; Chandy, K. G. Design of a potent and selective inhibitor of the intermediate-conductance  $Ca^{2+}$ -activated  $K^{+}$  channel, IK-Ca1: a potential immunosuppressant. *Proc. Natl. Acad. Sci. U.S.A.* **2000**, *97*, 8151–8156.
- Anaissie, E. J.; Vartivarian, S. E.; Abi-Said, D.; Uzun, O.; Pinczowski, H.; Kontoyiannis, D. P.; Khoury, P.; Papadakis, K.; Gardner, A.; Raad, I. I.; Gilbreath, J.; Bodey, G. P. Fluconazole versus amphotericin B in the treatment of hematogenous candidiasis: a matched cohort study. *Am. J. Med.* **1996**, *101*, 170–176.
- Bok, R. A.; Small, E. J. The treatment of advanced prostate cancer with ketoconazole: safety issues. *Drug Saf.* **1999**, *20*, 451–458.
- Nair, D. R.; Morris, H. H. Potential fluconazole-induced carbamazepine toxicity. *Ann. Pharmacother.* **1999**, *33*, 790–792.
- Jeng, M. R.; Feusner, J. Itraconazole-enhanced vincristine neurotoxicity in a child with acute lymphoblastic leukemia. *Pediatr. Hematol. Oncol.* **2001**, *18*, 137–142.
- Wolf, R.; Wolf, D.; Kuperman, S. Focal nodular hyperplasia of the liver after itraconazole treatment. *J. Clin. Gastroenterol.* **2001**, *33*, 418–420.
- Kauffman, C. A.; Hedderwick, S. A. Treatment of systemic fungal infections in older patients: achieving optimal outcomes. *Drugs Aging* **2001**, *18*, 313–323.
- Plempel, M. Experience, recognitions and questions in azole antimycotics. *Shinkin to shinkinsho* **1982**, *23*, 17–27.
- Fromling R. A. Overview of medically important antifungal azole derivatives. *Clin. Microbiol. Rev.* **1988**, *1*, 187–217.
- Ji, H.; Zhang, W.; Zhou, Y.; Zhang, M.; Zhu, J.; Song, Y.; Lü, J.; Zhu J. A three-dimensional model of lanosterol 14 $\alpha$ -demethylase of *Candida albicans* and its interaction with azole antifungals. *J. Med. Chem.* **2000**, *43*, 2493–2505.
- Podust, L. M.; Poulos, T. L.; Waterman, M. R. Crystal structure of cytochrome P450 14 $\alpha$ -sterol demethylase (CYP51) from mycobacterium tuberculosis in complex with azole inhibitors. *Proc. Natl. Acad. Sci. U.S.A.* **2001**, *98*, 3068–3073.
- InsightII 2000: Molecular Simulation Inc., 9685 Scranton Road, San Diego, CA 92121-3752.
- SYBYL 6.2: Tripos Associates, Inc., 1699S. Hanley Road, Suite 303, St. Louis, MO 63144.
- Frisch, M. J.; Trucks, G. W.; Schlegel, H. B.; Scuseria, G. E.; Robb, M. A.; Cheeseman, J. R.; Zakrzewski, V. G.; Montgomery, J. A., Jr.; Stratmann, R. E.; Burant, J. C.; Dapprich, S.; Millam, J. M.; Daniels, A. D.; Kudin, K. N.; Strain, M. C.; Farkas, O.; Tomasi, J.; Barone, V.; Cossi, M.; Cammi, R.; Mennucci, B.; Pomelli, C.; Adamo, C.; Clifford, S.; Ochterski, J.; Petersson, G. A.; Ayala, P. Y.; Cui, Q.; Morokuma, K.; Malick, D. K.; Rabuck, A. D.; Raghavachari, K.; Foresman, J. B.; Cioslowski, J.; Ortiz, J. V.; Stefanov, B. B.; Liu, G.; Liashenko, A.; Piskorski, P.; Komaromi, I.; Gomperts, R.; Martin, R. L.; Fox, D. J.; Keith, T.; Al-Laham, M. A.; Peng, C. Y.; Nanayakkara, A.; Gonzalez, C.; Challacombe, M.; Gill, P. M. W.; Johnson, B. G.; Chen, W.; Wong, M. W.; Andres, J. L.; Head-Gordon, M.; Replogle, E. S.; Pople, J. A. *Gaussian 98*, revision A.7; Gaussian, Inc.: Pittsburgh, PA, 1998.
- Cafilisch, A.; Miranker, A.; Karplus, M. Multiple copy simultaneous search and construction of ligands in binding sites: application to inhibitors of HIV-1 aspartic proteinase. *J. Med. Chem.* **1993**, *36*, 2142–2167.
- Evensen, E. R.; Joseph-McCarthy, D.; Karplus, M. *MCSS*, version 2.1; Harvard University, Cambridge, MA, 1997.
- Böhm, H.-J. The computer program LUDI: a new method for the de novo design of enzyme inhibitors. *J. Comput.-Aided Mol. Des.* **1992**, *6*, 61–78.
- Joseph-McCarthy, D.; Tsang, S. K.; Filman, D. J.; Hogle, J. M.; Karplus, M. Use of MCSS to design small targeted libraries: application to picornavirus ligands. *J. Am. Chem. Soc.* **2001**, *123*, 12758–12769.
- Luty, B. A.; Wasserman, Z. R.; Stouten, P. F. W.; Hodge, C. N.; Zacharias, M.; McCammon, J. A. A molecular mechanics/grid method for evaluation of ligand–receptor interactions. *J. Comput. Chem.* **1995**, *16*, 454–464.
- Böhm, H.-J. The development of a simple empirical scoring function to estimate the binding constant for a protein–ligand complex of known three-dimensional structure. *J. Comput.-Aided Mol. Des.* **1994**, *8*, 243–256.
- Böhm, H.-J. Prediction of binding constants of protein ligands: A fast method for the prioritization of hits obtained from de novo design or 3D database search programs. *J. Comput.-Aided Mol. Des.* **1998**, *12*, 309–323.
- Aoyama, Y.; Kudo, M.; Asai, K.; Okonogi, K.; Horiuchi, T.; Gotoh, O.; Yoshida, Y. Emergence of fluconazole-resistant sterol 14-demethylase P450 (CYP51) in *Candida albicans* is a model demonstrating the diversification mechanism of P450. *Arch. Biochem. Biophys.* **2000**, *379*, 170–171.
- Aoyama, Y.; Yoshida, Y.; Sato, R. Yeast cytochrome P-450 catalyzing lanosterol 14 $\alpha$ -demethylation. *J. Biol. Chem.* **1984**, *259*, 1661–1666.
- Nitahara, Y.; Kishimoto, K.; Yabusaki, Y.; Gotoh, O.; Yoshida, Y.; Horiuchi, T.; Aoyama, Y. The amino acid residues affecting the activity and azole susceptibility of rat cyp51 (sterol 14-demethylase P450). *J. Biochem.* **2001**, *129*, 761–768.
- Hasemann, C. A.; Kurumbail, R. G.; Boddupalli, S. S.; Peterson, J. A.; Deisenhofer, J. Structure and function of cytochromes P450: a comparative analysis of three crystal structures. *Structure* **1995**, *2*, 41–62.
- Schlichting, I.; Berendzen, J.; Chu, K.; Stock, A. M.; Maves, S. A.; Benson, D. E.; Sweet, R. M.; Ringe, D.; Petsko, G. A.; Sligar, S. G. The Catalytic Pathway of Cytochrome P450cam at Atomic Resolution. *Science* **2000**, *287*, 1615–1622.
- Lewis, D. F. V.; Wiseman, A.; Tarbit, M. H. Molecular modelling of lanosterol 14 $\alpha$ -demethylase (CYP51) from *Saccharomyces cerevisiae* via homology with CYP102, a unique bacterial cytochrome P450 isoform: quantitative structure–activity relationships (QSARs) within two related series of antifungal azole derivatives. *J. Enzyme Inhib.* **1999**, *14*, 175–192.
- Yoshida, Y.; Imai, Y.; Hashimoto-Yutsudo, C. Spectrophotometric examination of exogenous-ligand complexes of ferric cytochrome P-450. Characterization of the axial ligand trans to thiolate in the native ferric low-spin form. *J. Biochem.* **1982**, *91*, 1651–1659.